CRYSTAL GROWTH & DESIGN

pubs.acs.org/crystal

Article

Selective Area Epitaxy of GaN Nanostructures: MBE Growth and Morphological Analysis

Syed M. N. Hasan, Weicheng You, Arnob Ghosh, Sharif Md. Sadaf,* and Shamsul Arafin*

Cite This: *Cryst. Growth Des.* 2023, 23, 4098−4104

Read Online

ACCESS | Metrics & More | Article Recommendations

ABSTRACT: This work presents the selective area epitaxy of GaN nanostructures grown on Ga-polar GaN/sapphire substrates by plasma-assisted molecular beam epitaxy. We demonstrate three types of nanostructures, including nanowires, nanofins, and nanorings on GaN-on-sapphire templates as well as investigate the ways of controlling their morphology, and orientation of sidewall plus top facets. A range of growth conditions including low to high Ga flux were employed during selective area epitaxy to develop these nanostructures with homogenous geometry and near vertical and smooth sidewalls. Using appropriate growth conditions and mask patterning orientations, nonpolar nanofin grids containing both/either *m*-/*a*-planes with as low as 260 nm fin width and up to six interconnects are demonstrated with smooth sidewalls. Based on these experimental results, we developed a growth model that takes different sidewall facets and orientations into account. The model generalizes the experimental results well and explains the growth conditions for the nanostructures. This study serves to advance the understanding of selective area epitaxy for defining complex III-nitride nanostructures that constitute an active area of research and development in the fields of nanotechnology and nanoscience.

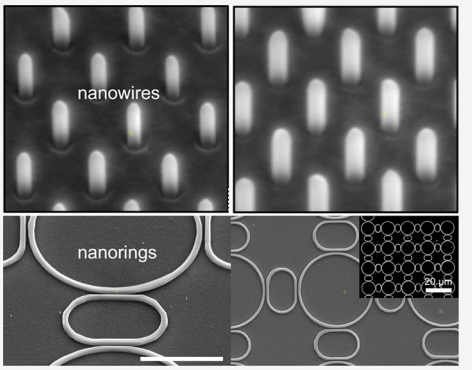

1. INTRODUCTION

Group III-nitride nanostructures have emerged as a promising platform for a number of application areas including optoelectronics,[1−4] power electronics,[5] sensing,[6,7] and photocatalysis.[8,9] In the optoelectronics area, such nanostructures are useful for both classical- and quantum-photonic devices operating at a wide spectral range.[10−12] Plasma-assisted molecular beam epitaxy (PAMBE) is one of the popular methods of growing nanostructures fabricated by self-assembly[13,14] under nonequilibrium growth conditions. Although self-assembled epitaxy can be performed on various low-cost substrates with a significantly large lattice mismatch, such nanostructures preferentially grow in polar *c*-directions and result in random nucleation with a large density of point defects.[15] Moreover, it is fundamentally challenging to control the size, shape, position, growth direction (both lateral and vertical), and density of the nanostructures.[16] The preferential growth along the axial *c*-direction and the spatial and structural variations of nanostructures primarily present a challenge for device fabrication and further limits their usage in device applications.[13,14,17] Self-assembled III-nitride nanostructures have been extensively studied for both material characterization and fabricating associated devices. The previously reported works are, however, still limited to nanowires (often termed as 1D structures).

Selective area epitaxy (SAE)[18,19] is a viable alternative to precisely control the size, position, shape, and density with an added advantage of controllability on III-nitride crystal planes, such as polar, semipolar and nonpolar facets of nanostructures.[20−23] The powerful SAE technique yields various types of nanostructures ranging from nanowires (NWs), nanofins (NFs), and nanorings (NRs). Until recently, it has remained challenging to understand the SAE kinetics and selectively grow nanostructures using different mask materials. The growth window (growth temperature and metal and N-fluxes), choices of substrates, and masks for SAE remain narrow. Due to anisotropic physical properties including various free surface energies and related direction-dependent growth rates, SAE has remained challenging. Additionally, achieving device-quality SAE-grown nanostructures are handicapped by surface roughness, the emergence of large semipolar planes due to a low growth rate,[24,25] distorted sidewalls,[23] and the inability to fill up closely-packed nanostructured openings.[26]

There have been very few reports on the SAE epitaxy of GaN nanostructures including NWs, NFs, and NRs. Engineering the sidewall facets of both NW- and NF-type structures by

Received: December 20, 2022
Revised: May 5, 2023
Published: May 16, 2023

https://doi.org/10.1021/acs.cgd.2c01506
Cryst. Growth Des. 2023, 23, 4098−4104

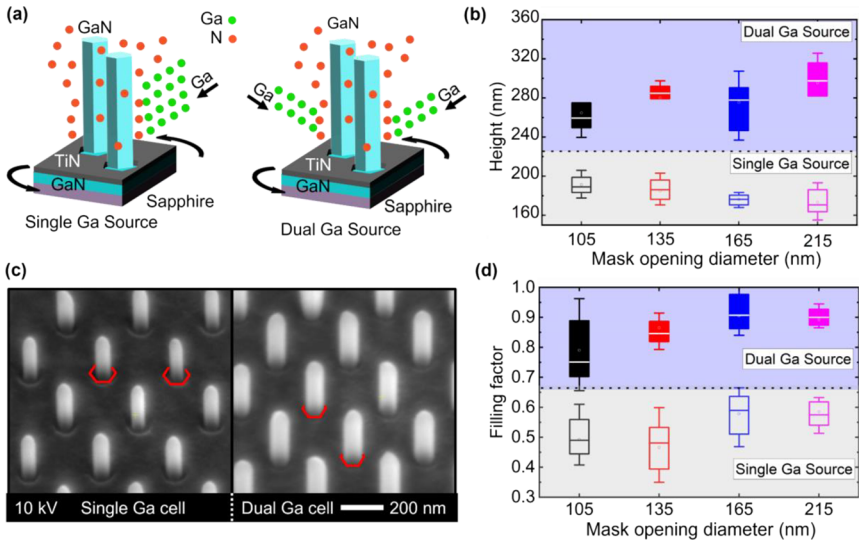

Figure 1. (a) Schematic view of Ga flux exposure by single and dual Ga effusion cells, for NWs grown by single and dual Ga effusion cells, (b) height of NWs in dependence on mask opening diameter, (c) 45° view of NWs with a mask opening diameter of 105 nm, and (d) NW filling factor as a function of mask opening diameter.

varying the Ga- and N-fluxes in MBE was reported.[27] Controlling the sidewall roughness and complete coverage of the nano-openings by SAE was also recently achieved.[28] Despite the developments, SAE GaN structures are still restricted to only NWs and NFs types with sidewall planes from a single family to mixed *m*- and/or *a*-planes. To our best knowledge, there are no reports on the SAE of complex structures such as interconnects and ring patterns on III nitrides. SAE growths of interconnects and fins require extensive studies as the growth kinetics becomes complex due to multiple nucleation sites and coalescence/merging.[29] The coalescence/merging process and crystal orientation of the nanostructure branches determine the crystal phase and often demonstrates defect generation.[30]

In this study, we investigate the SAE of the aforementioned nanostructures under three different Ga-rich conditions, such as low, intermediate, and high. Single- and double Ga cells were used during the growth to control their morphology and crystal planes. The as-grown nanostructures exhibit excellent selectivity and surface smoothness. Three different nanostructures, such as (i) NWs, (ii) NFs, and (iii) NRs were systematically studied, the effects of Ga:N flux ratios on growth kinetics as well as the evolution of polar, nonpolar, and semipolar facets were investigated. The dependencies of incomplete filling of the GaN nanostructures, growth rate as well as sidewall morphology on Ga adatom distribution are discussed. By adjusting Ga:N flux ratios, we control the sidewall morphology for both NWs and NFs and determine the appropriate growth condition for each of these nanostructures. With careful optimization of our growth process, we develop nanostructures with dimensions <300 nm and ultra-smooth sidewalls. Hence, SAE-grown three-dimensional GaN nanostructures - wires, fins, rings, and curved features enable the fabrication of a wider range of electronic and photonic devices, such as fin field-effect transistors, lasers, and light-emitting diodes (LEDs).[18,19,23,31]

2. EXPERIMENTAL DESCRIPTIONS

The GaN nanostructures studied in this work were selectively grown on GaN-on-sapphire templates using a Veeco GEN 930 PAMBE system. Prior to SAE, 20 nm of Ti, serving as a hard mask during growth, was evaporated on the templated substrates. Different shaped nano-openings were then defined using electron beam lithography (EBL) and subsequent dry etching. Hexagonal nano-openings with various diameters and spacings (pitch 150−300 nm) in a periodical honeycomb arrangement as well as fin structures with widths in the range of 150−250 nm were fabricated. The patterned substrates were then loaded into the MBE reactor, followed by a buffer bake at 400 °C for 1 h. Prior to the growth, Ti was transformed into amorphous TiN. This was done by nitridating the substrates with N_2 plasma at a forward RF plasma power of 300 W and a nitrogen flow rate of 2 sccm for 10 min at a thermocouple temperature of 500 °C and 3 min at 800 °C. To promote growth selectivity and/or Ga desorption from Ti-mask surface to prevent any parasitic GaN growth on Ti mask, SAE is usually performed at a relatively higher temperature compared to self-assembled growth.[32] Therefore, undoped GaN was grown over a 2 h period at a thermocouple temperature of 850 °C. To ensure uniform flux distribution, the samples were rotated at 1 rpm during the growth. Ga fluxes were varied in the range of 2×10^{-7} to 7.7×10^{-7} Torr beam equivalent pressure (BEP) with a fixed N_2 flow. A Thermo Scientific Quattro environmental scanning electron microscope (SEM) at an accelerating voltage of 10 kV was then used to determine the morphology of the as-grown samples under study. To evaluate the crystal quality of the as-grown nanostructures, high-resolution transmission electron microscopy (HR-TEM) was carried out on an FEI Titan 80-300 analytical transmission electron microscope equipped with an EDAX Octane Elite energy-dispersive x-ray spectrometer.

3. RESULTS AND DISCUSSION

Understanding the influence of growth temperature, Ga flux, and Ga/N ratio on the realization of GaN nanostructures is of utmost importance. The following subsections describe the formation of GaN NWs, NFs, and NRs, the required growth conditions of these nanostructures and their morphology plus facet orientations are carefully examined. Based on our observations, a growth model is proposed at the end.

3.1. Formation of Nanowires. *3.1.1. Effect of Dual Ga Effusion Cells.* A high Ga:N ratio, i.e., a Ga-rich condition was adopted previously to maintain axial growth despite Ga desorption and GaN decomposition.[24,27] Achieving a high Ga density is important to achieve large-area growth with minimum size variation arising from the shadow effect or

https://doi.org/10.1021/acs.cgd.2c01506
Cryst. Growth Des. 2023, 23, 4098−4104

optimum filling of nano-opening.[26] Supplying a high-density of Ga adatoms to promote their uniformity and achieve higher growth rates requires the involvement of multiple Ga effusion cells. Therefore, dual Ga cells were simultaneously used with a combined Ga flux of 5.4×10^{-7} Torr BEP, split equally into two cells to grow GaN NWs, as schematically shown in Figure 1a. For comparison, another sample was grown with a similar Ga flux but supplied by a single cell while keeping the remaining growth conditions the same.

With the use of dual Ga cells, growth rates of GaN are found to drastically improve from 1.6 nm/min while using a single Ga cell to 2.2 nm/min (for nano-opening array with 105 nm diameter). A change in the growth rate with changing mask opening diameter is observed on both the samples, while the dual Ga cell sample maintains its higher growth rate irrespective of the nano-opening dimensions as shown in Figure 1b. Regardless of the number of Ga cells used, good selectivity was maintained along the entire sample, and hexagonal NWs with *m*-side planes are seen. The hexagonal shape of the NWs also indicates that Ga-rich conditions were maintained since N-rich growth otherwise creates irregular-shaped nanostructures.

Besides the increase of growth rates, improved Ga distribution significantly enhances the nano-opening coverage by the grown NWs. The red marks around the hexagonal nano-opening on the Ti mask as shown in Figure 1c indicate that the grown NWs have a smaller diameter compared to the nano-opening when a single Ga cell was used. The SEM images of the NW dimensions reveal the strong dependence of NW height on Ga flux distribution. Figure 1d shows the filling factor, defined as the ratio of the cross-sectional area of NWs to nano-openings, as a function of nano-opening diameters. In contrast to N radicals which get incorporated immediately at appropriate crystal sites, or otherwise form molecular N_2, Ga adatoms remain mobile within their diffusion lengths before reaching the nano-openings or desorbed. As it appears from Figure 1d, Ga adatoms reaching the nano-opening increase at a higher order while using multiple cells, despite using the same amount of Ga fluxes. Ga adatoms supplied by a single cell fill <60% of the nano-openings even for larger openings, which only reduces further as the dimensions become smaller. It is worth mentioning for all samples, the spacing between the NWs was fixed at 200 nm for these calculations. For NWs with smaller diameter, more NWs can be placed in a fixed area. The higher number of NWs causes the Ga collection area (area with Ga diffusion length as radius) to overlap, which in turn reduces the amount of Ga per nano-opening. However, as it appears, a redistribution of Ga adatoms using dual cells increased both the growth rate and NW diameter. Simultaneous improvement on both *c*- and *m*-plane indicates the Ga density around the NWs increases since Ga adatoms residing on the *m*-planes are responsible for increasing the NW dimension laterally, while the adatoms over the *c*-plane increase NW height.

3.1.2. Impact of Ga:N Ratios. To further understand the impact of Ga flux (or Ga:N ratio) on NWs using dual Ga cells, a series of Ga flux was tested while keeping the N-plasma condition unchanged. We explored low Ga:N (N-rich) to high Ga:N (Ga-rich) ratios and systematically analyzed the impact by observing both NWs and NFs. Figure 2 shows the impact of Ga flux over NW morphology. For each sample, NWs with four different diameters were analyzed. The NW dimensions including both height and sidewall facets were found to be

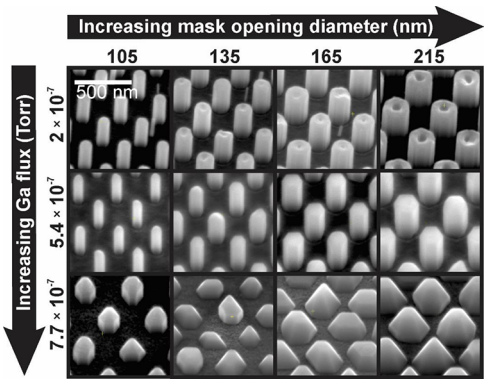

Figure 2. 45°-tilted view of GaN NWs grown with Ga fluxes in the range of 2×10^{-7}–7.7×10^{-7} Torr (top to bottom). The nano-opening diameter is increased from left to right. All NWs have a 200 nm pitch distance.

heavily dependent on Ga fluxes. The smooth *m*-plane sidewalls with flat *c*-plane top found for the sample grown with a Ga flux of 5.4×10^{-7} Torr quickly disappears as the Ga flux is changed in either higher flux or lower. The NW morphology, however, is drastically different. Based on our analysis, we found that high Ga flux promotes the semipolar growth of *r*-planes and lateral spreading of GaN over the mask, while growth along the *c*-plane and *m*-plane is suppressed. This happens because the SAE growth of GaN NWs significantly depends on Ga adatom diffusion/desorption on the sidewalls, which is affected in the presence of high Ga flux. On the other hand, when lower Ga fluxes were used, distorted NWs containing inhomogeneous top facet with no apparent *m*-/*a*-plane side facets are found. Furthermore, instead of solid columnar structures, a hollow core shape (nanotube-like) is observed which is shown in the top row of Figure 2. The incomplete coverage of the nano-opening or the hollow area at the center of the NW kept increasing as the NW diameter increases. The growth of a nanotube structure instead of an NW is attributed to lower Ga fluxes. Due to the significant lowering of Ga flux, the growth condition switched from Ga-rich to N-rich. With limited Ga flux, the effective Ga adatom diffusion significantly reduces and the adatoms bonded with N species immediately as it reaches the nano-opening perimeter. By densely populating patterns with small periods, such hollow structures were also previously reported and attributed to the local transition from Ga-rich to N-rich growth conditions.[18,26] Since N radicals also promote GaN formation, parasitic GaN formation over the TiN mask is observed for this sample. Thus, growth selectivity is also affected by the change in Ga:N ratios.

Interestingly, the NW growth rate is recorded to be the highest for the lowest supply of Ga fluxes, 2×10^{-7} Torr (see Figure 3a). Under Ga-rich conditions, the initial growth stage involves the formation of multiple seed layers and their eventual coalescence into each other to fill up the nano-opening before NW grows vertically. In contrast, under N-rich conditions, multiple NWs start to grow in each opening, preferably on the edge of the nano-openings and coalescence happens much later in the growth process. This leads to distorted NW side faces the absence of any *m*-planes, and high growth rate since the seed NWs are often relatively small in diameter. As the Ga flux increases to a nominal condition, the hollow shapes transform into a filled NW. The presence of Ga adatoms at both *m*- and *c*-planes results in reduced NW height but with a homogenous hexagonal shape with smooth

https://doi.org/10.1021/acs.cgd.2c01506
Cryst. Growth Des. 2023, 23, 4098−4104

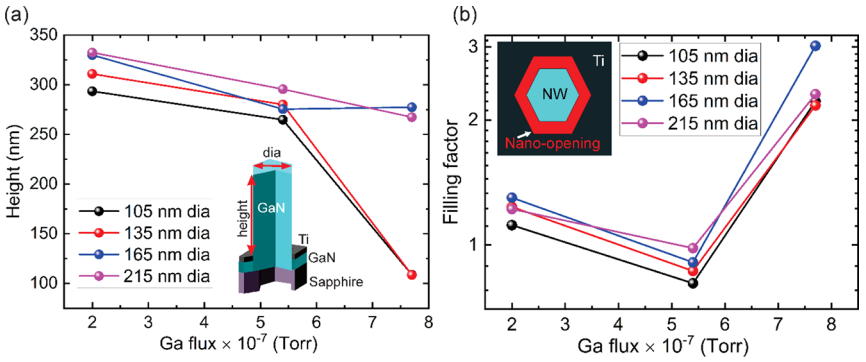

Figure 3. NWs with (a) height and (b) filling factor as a function of Ga fluxes with varying mask opening diameters. All NWs are spaced 200 nm apart.

sidewalls. The filling factor also reveals that the distorted nanocolumns are slightly larger than the nano-openings (>1), which becomes ∼1 as the Ga flux reaches 5.4×10^{-7} Torr. As the low Ga flux promotes vertical growth, the high Ga flux (7.7×10^{-7} Torr) promotes semipolar growth which has a much slower growth rate. As can be seen in Figure 2, the NWs grown at high Ga fluxes emerged as pyramidal shape confined mostly by a semipolar *r*-plane with very small *m*-plane sidewall facets and no flat-*c*-plane at the top. The average NW height at such high Ga flux reduced to about half the height of the NWs grown with 5.4×10^{-7} Torr Ga flux, while the diameter increased ∼2.7 times compared to the latter. The slower growth rate on the semipolar facets along with a large amount of Ga adatom on the sidewalls caused significant overgrowth on the mask, yielding a filling factor > 1 (see Figure 3b) which nearly caused coalescence between neighboring NWs for nano-openings with a diameter of >165 nm.

3.2. Formation of Nanofins. We then applied the developed Ga flux control technique to form complex NFs using SAE. Fabricating NFs with *m*-/*a*-planes is easier since the in-plane crystal orientation is guided by mask patterns. However, the development of NFs involves the merging/coalescence of multiple fins which could lead to defect formation. Hence, the morphological evaluation of NFs is important in realizing complex NF interconnects.

Figure 4 presents different NF shapes grown with Ga fluxes of 7.7×10^{-7} and 5.4×10^{-7} Torr. Interestingly, the reduced axial- and large lateral overgrowth attained for the NWs while growing at 7.7×10^{-7} Torr Ga flux are not observed in NFs. Smooth, near-vertical sidewalls with no visible defects over the top *c*-plane are found. In contrast, a slightly less Ga flux 5.4×10^{-7} Torr used for the homogenous NW growth with smooth sidewalls and homogenous top surface provided defects lines and discontinuity on the top *c*-plane with nonuniform fin width. All of which disappear with a higher Ga flux. The difference in the morphology between NWs and NFs is mainly due to their different geometry. Compared to NWs, NFs possess a significantly larger surface area. This high surface area reduces the Ga adatom density present on the sidewalls and promotes desorption instead of enhancing lateral overgrowth. Thus, the higher Ga flux mostly impacts the top surface/*c*-plane facets and creates a homogeneous, flat top surface, absent of any discontinuities. We inspected the interconnects of six junctions for both *a*-/*m*-plane families. Compared to *a*-planes, GaN NFs with *m*-plane sidewalls were uniform for both samples. Theoretical calculations show that *m*-plane GaN has

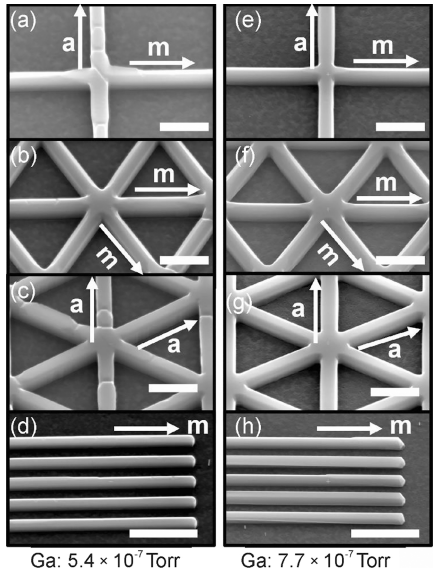

Figure 4. 45°-tilted SEM images of nanofins grown with varying Ga fluxes. (a–d) NF grown at 5.4×10^{-7} Torr Ga flux, (e–h) NFs grown at 7.7×10^{-7} Torr Ga flux. From top to bottom, quadrangular nanofin consisting of *a*- and *m*-planes, symmetrical junction of *m*-plane family orientation, symmetrical junction of *a*-plane family orientation, and NFs with *m*-plane sidewalls with 230 nm width and 500 nm spacing. All scale bars represent 1 μm length if not mentioned otherwise.

lower surface energy compared to *a*-planes, making *m*-planes more energetically favorable.[33]

It was reported that *a*-plane GaN has a larger density of surface states than *m*-plane GaN.[34] Because of such a higher density of states, *a*-planes offer more Ga adsorption sites which results in a reduced Ga adatom mobility.[34] Because *a*-plane is not energetically favorable, polygonal GaN nanostructures with mixed *m*- and *a*-planes evolve while growing along *a*-planes. While other reports presented significant sidewall roughness and faceted morphology along the *a*-plane structures,[28] much less sidewall defects are found in our sample. Nonetheless, the growth rates along these planes are different, coalescence/merging of the mixed crystal planes created a notch-like morphology visible from the top facet (Figure 4a,c). As the Ga flux increases, such surface morphologies are either covered up by excess GaN growth or are not created in the first place due to higher Ga adatom interactions. In either case, complex NF structures with quadrangular junctions, and interconnects with as high as six junctions are implemented using dual Ga cell combination.

https://doi.org/10.1021/acs.cgd.2c01506
Cryst. Growth Des. 2023, 23, 4098−4104

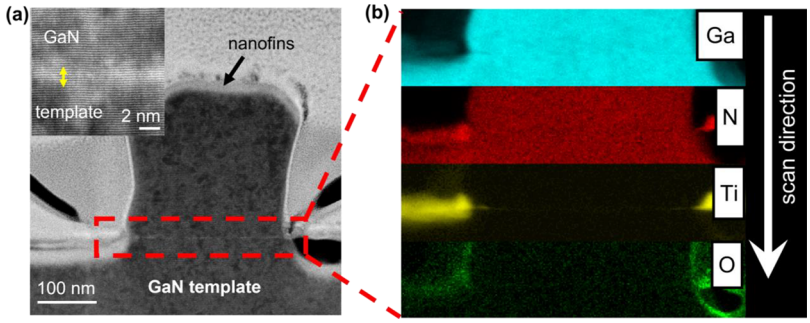

Figure 5. (a) Cross-sectional HRTEM image and (b) EDS mapping of a nanofin structure grown with dual-cell 7.7 × 10^{-7} Torr Ga flux.

Figure 5a represents the cross-sectional TEM image of the GaN NFs grown at a Ga flux of 7.7 × 10^{-7} Torr, (see Figure 4). No observable dislocations or defect lines are seen, indicating that no defects are generated or transferred from the underlying substrates. An atomically sharp interface between the GaN templates and the grown materials, as shown in the inset, was also observed. STEM energy-dispersive X-ray spectroscopy (EDS) was conducted to investigate the possible contamination at the GaN template/nanostructure growth interface, as shown in Figure 5b. The electron beam was moved in a vertical line across the regrowth interface to produce a relative concentration profile. Several EDS scans were performed in various locations of the sample, and trace amounts of Ti were found. This problem may be caused by the insufficient etching of the Ti mask. Nonetheless, a thorough inspection of the interface and surrounding layers reveal uniform growth of the epilayers, with no discontinuities, indicating that a small amount of Ti may not have played a crucial role in the growth. However, to avoid such issues, proper clearing procedures will be followed in future growth.

3.3. Formation of Nanorings. Figure 6 shows the 45°-tilted and top-views of the NRs grown with 7.7 × 10^{-7} Torr Ga

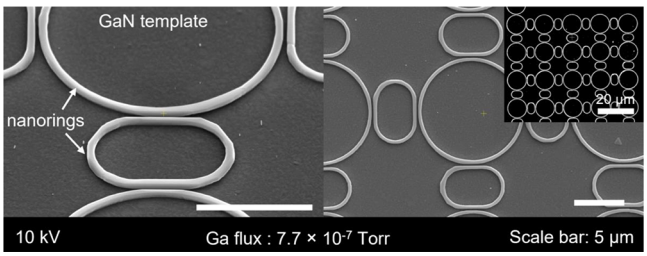

Figure 6. SEM images of the nanorings. A ring array to realize complex photonic devices is shown as an inset.

flux under otherwise identical conditions. As can be seen, the NRs followed the growth morphology of the NFs instead of NWs and near vertical sidewalls are achieved. While smooth sidewalls were maintained throughout the ring, some mixed planes and notches are observed as the rings started to change the plane and along the minor axis, which is orthogonal to the *a*-directions, resulting in *a*-plane sidewalls. Interestingly, no structural discontinuity is found for the NRs, despite small widths (260 nm) and large diameters (5/10 μm) and narrow coupling gaps (200 nm) in the structures. The inset of Figure 6 shows the 50 μm × 50 μm area of the ring structures, free of any distorted patterns as well as any parasitic GaN formations on the TiN mask. Our approach involving dual Ga cells and a high Ga:N ratio proves effective to achieve large-area NRs with realistic dimensions. This opens the possibility to realize passive photonic components, such as low-loss waveguides, ring resonators, and ring arrays. Thanks to SAE which could generate these nanoscale complex patterns without major fabrication efforts toward making useful photonic devices.

3.4. Growth Model. Based on our Ga flux series, NWs and NFs show different morphologies while changing the Ga flux from intermediate (5.4 × 10^{-7} Torr) to high flux (7.7 × 10^{-7} Torr) conditions. With increasing Ga flux, NWs exhibit an accelerated growth of lateral *m*-/*a*-planes compared to the vertical *c*-plane. This can be explained by the difference in the Ga atoms' adsorption/desorption behavior between the polar and nonpolar planes. Schematically shown in Figure 7, as the

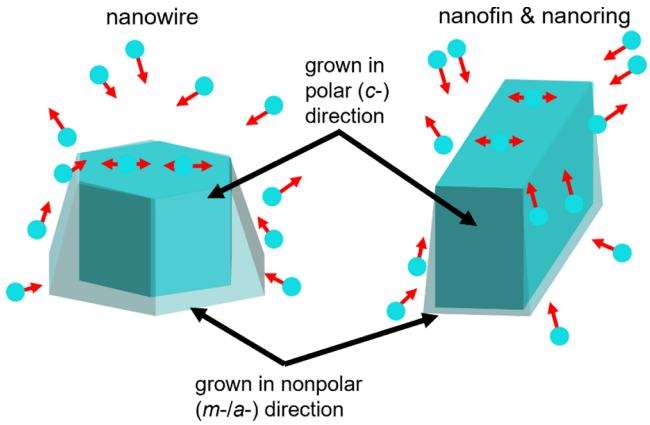

Figure 7. Schematic representation of different growth conditions for NWs and NFs-NRs with both *c*-plane and *m*−/*a*-planes.

growth proceeds, Ga adatoms reach the nanostructures in two ways, i) direct impingement of Ga atoms on the growth structures from the effusion cells and ii) traveling of the Ga adatoms from the mask surface to within their diffusion lengths toward the nanostructures. These diffused adatoms travel along the sidewalls and are incorporated on the *m*-/*a*-planes, and at the top *c*-plane. With high Ga fluxes, the number of Ga adatoms reaching the NW sidewalls is much higher, which gives rise to a significant lateral growth rate and results in a truncated pyramid shape. Such lateral spreading is expected to be reduced for the NFs since the nonpolar planes promote desorption. In fact, the desorption rate of Ga adatoms on the *m*-planes was found to be nearly two times higher than on the *c*-planes.[35] It was also observed that the sticking coefficient of Ga adatoms was lower in *m*-planes than in *c*-planes.[36] Ga adatoms also redistribute themselves around the large sidewalls for both the NFs and NRs, reducing overall Ga adatom density

https://doi.org/10.1021/acs.cgd.2c01506
Cryst. Growth Des. 2023, 23, 4098−4104

on the sidewalls. This, along with a higher desorption rate proves beneficial to stop lateral spreading for our NFs. The higher sticking coefficient on the *c*-planes also ensures Ga adatoms travel from the sidewalls to the top facets and they remain on the *c*-plane, further increasing axial growth.

As stated earlier, NFs possess considerably a larger sidewall area compared to NWs. This increased aspect ratio changes the Ga:N ratio locally for densely packed NF designs. By comparing the nano-opening surface area with the sidewall area, NFs have a higher sidewall area (also higher Ga collection area) compared to NWs and as a result, the NF sidewalls absorb the Ga adatoms more. Hence, the Ga adatom density reduces at the bottom of densely packed structures, leading to local N-rich growth conditions.[18,23] Since the N-rich condition suppresses lateral growth, the NFs become more vertical.[27] In our experiments, both NFs and NRs demonstrate near-vertical sidewalls despite much different spacing between neighboring structures (NF ∼1.5 μm and NR 0.3−5 μm). Thus, Ga-rich conditions are expected to be maintained over the entire growth surface and the vertical sidewall is due to the redistribution of Ga adatoms over a large area. In addition to the qualitative model discussed above, there are also quantitative models that consider Ga/N flux ratio, growth temperature, and template geometry.[20,37,38] It was reported in the quantitative growth model[37] that the dimensions and pitch of the nanopattern heavily influence the selectivity for a specific growth condition.

4. CONCLUSIONS

In summary, we make a detailed investigation of the SAE of GaN nanostructures grown on Ga-polar GaN/sapphire substrates by PAMBE. Three different types of bulk-like nanostructures (which could be termed as quasi-3D structures since no reduced dimensionality in either direction) are demonstrated using the bottom-up growth approach. It is found that the use of two simultaneous gallium effusion cells contributes to achieve homogenous NWs with a cross-sectional area equal to the nano-openings. The increases in growth rates employing dual Ga effusion cells for a given flux open the possibilities to develop nanostructures with a large aspect ratio. We also define GaN NFs with up to six interconnects as well as NRs with improved sidewall facets and top facet morphology. Since the formation of GaN nanostructures by SAE is still at a preliminary stage, further efforts need to be made by growing useful InGaN/GaN heterostructures with similar growth selectivity. Growing *p-i-n* diode nanostructures using SAE for micro-LEDs or advanced light sources is beyond the scope of this work and will be done in our future studies. Hence, the formation of complex nanostructures reported here is an essential step toward the implementation of next-generation electronic and optoelectronic devices in both classical and quantum areas.

AUTHOR INFORMATION

Corresponding Authors

Sharif Md. Sadaf − *Centre Energie, Matériaux et Télécommunications, Institut National de la Recherche Scientifique (INRS)-Université du Québec, Varennes, Quebec J3X 1S2, Canada*; Email: sharif.sadaf@inrs.ca

Shamsul Arafin − *Department of Electrical and Computer Engineering, The Ohio State University, Columbus, Ohio 43210, United States*; orcid.org/0000-0003-4689-2625; Email: arafin.1@osu.edu

Authors

Syed M. N. Hasan − *Department of Electrical and Computer Engineering, The Ohio State University, Columbus, Ohio 43210, United States*

Weicheng You − *Department of Electrical and Computer Engineering, The Ohio State University, Columbus, Ohio 43210, United States*

Arnob Ghosh − *Department of Electrical and Computer Engineering, The Ohio State University, Columbus, Ohio 43210, United States*

Complete contact information is available at: https://pubs.acs.org/10.1021/acs.cgd.2c01506

Notes

The authors declare no competing financial interest.

ACKNOWLEDGMENTS

This research was funded by the National Science Foundation (NSF) under grant number 2020015. Electron microscopy was performed at the Center for Electron Microscopy and Analysis (CEMAS) at The Ohio State University. This work was also partially supported by the NSERC Discovery Grant program. The authors would like to acknowledge Matthew M. Schneider and John Watt, members of the Materials Science and Technology Division and Center for Integrated Nanotechnologies, respectively, within Los Alamos National Laboratory, Los Alamos, NM 87545, USA, for performing transmission electron microscopy. Electron microscopy was also performed, in part, at the Center for Integrated Nanotechnologies, an Office of Science User Facility operated by the U.S. Department of Energy (DOE) Office of Science. Los Alamos National Laboratory, an affirmative action equal opportunity employer, is managed by Triad National Security, LLC for the U.S. Department of Energy's NNSA, under contract 89233218CNA000001.

REFERENCES

(1) Guo, W.; Zhang, M.; Banerjee, A.; Bhattacharya, P. Catalyst-free InGaN/GaN nanowire light emitting diodes grown on (001) silicon by molecular beam epitaxy. *Nano Lett.* **2010**, *10*, 3355−3359.

(2) Koester, R.; Sager, D.; Quitsch, W.-A.; Pfingsten, O.; Poloczek, A.; Blumenthal, S.; Keller, G.; Prost, W.; Bacher, G.; Tegude, F.-J. High-speed GaN/GaInN nanowire array light-emitting diode on silicon (111). *Nano Lett.* **2015**, *15*, 2318−2323.

(3) Yi, W.; Uzuhashi, J.; Chen, J.; Kimura, T.; Kamiyama, S.; Takeuchi, T.; Ohkubo, T.; Sekiguchi, T.; Hono, K. Cathodoluminescence and scanning transmission electron microscopy study of InGaN/GaN quantum wells in core-shell GaN nanowires. *Appl. Phys. Express* **2019**, *12*, No. 085003.

(4) Hasan, S. M.; You, W.; Sumon, M. S. I.; Arafin, S. Recent progress of electrically pumped AlGaN diode lasers in the UV-B and-C bands. *Photonics* **2021**, *8*, 267.

(5) Huang, Y.-P.; Hsu, W.-C.; Liu, H.-Y.; Lee, C.-S. Enhancement-mode tri-gate nanowire InAlN/GaN MOSHEMT for power applications. *IEEE Electron Dev. Lett.* **2019**, *40*, 929−932.

(6) Maier, K.; Helwig, A.; Müller, G.; Schörmann, J. r.; Eickhoff, M. Photoluminescence detection of surface oxidation processes on InGaN/GaN nanowire arrays. *ACS Sens.* **2018**, *3*, 2254−2260.

(7) Teubert, J.; Becker, P.; Furtmayr, F.; Eickhoff, M. GaN nanodiscs embedded in nanowires as optochemical transducers. *Nanotechnology* **2011**, *22*, No. 275505.

(8) Kibria, M. G.; Edwards, J. P.; Gabardo, C. M.; Dinh, C. T.; Seifitokaldani, A.; Sinton, D.; Sargent, E. H. Electrochemical CO2 reduction into chemical feedstocks: from mechanistic electrocatalysis models to system design. *Adv. Mater.* **2019**, *31*, No. 1807166.

(9) Kibria, M.; Chowdhury, F.; Zhao, S.; AlOtaibi, B.; Trudeau, M.; Guo, H.; Mi, Z. Visible light-driven efficient overall water splitting using p-type metal-nitride nanowire arrays. *Nat. Commun.* **2015**, *6*, 6797.
(10) Xiong, C.; Pernice, W. H.; Sun, X.; Schuck, C.; Fong, K. Y.; Tang, H. X. Aluminum nitride as a new material for chip-scale optomechanics and nonlinear optics. *New J. Phys.* **2012**, *14*, No. 095014.
(11) Deshpande, S.; Frost, T.; Hazari, A.; Bhattacharya, P. Electrically pumped single-photon emission at room temperature from a single InGaN/GaN quantum dot. *Appl. Phys. Lett.* **2014**, *105*, 141109.
(12) Arakawa, Y.; Holmes, M. J. Progress in quantum-dot single photon sources for quantum information technologies: A broad spectrum overview. *Appl. Phys. Rev.* **2020**, *7*, No. 021309.
(13) Sadaf, S.; Ra, Y.-H.; Nguyen, H.; Djavid, M.; Mi, Z. Alternating-current InGaN/GaN tunnel junction nanowire white-light emitting diodes. *Nano Lett.* **2015**, *15*, 6696−6701.
(14) Hasan, S. M.; Ghosh, A.; Sadaf, S. M.; Arafin, S. Effects of InGaN quantum disk thickness on the optical properties of GaN nanowires. *J. Cryst. Growth* **2022**, *588*, No. 126654.
(15) Fernández-Garrido, S.; Kong, X.; Gotschke, T.; Calarco, R.; Geelhaar, L.; Trampert, A.; Brandt, O. Spontaneous nucleation and growth of GaN nanowires: the fundamental role of crystal polarity. *Nano Lett.* **2012**, *12*, 6119−6125.
(16) Tourbot, G.; Bougerol, C.; Grenier, A.; Den Hertog, M.; Sam-Giao, D.; Cooper, D.; Gilet, P.; Gayral, B.; Daudin, B. Structural and optical properties of InGaN/GaN nanowire heterostructures grown by PA-MBE. *Nanotechnology* **2011**, *22*, No. 075601.
(17) Nami, M.; Stricklin, I. E.; DaVico, K. M.; Mishkat-Ul-Masabih, S.; Rishinaramangalam, A. K.; Brueck, S.; Brener, I.; Feezell, D. F. Carrier dynamics and electro-optical characterization of high-performance GaN/InGaN core-shell nanowire light-emitting diodes. *Sci. Rep.* **2018**, *8*, 501.
(18) Winnerl, J.; Kraut, M.; Artmeier, S.; Stutzmann, M. Selectively grown GaN nanowalls and nanogrids for photocatalysis: growth and optical properties. *Nanoscale* **2019**, *11*, 4578−4584.
(19) Pantle, F.; Becker, F.; Kraut, M.; Wörle, S.; Hoffmann, T.; Artmeier, S.; Stutzmann, M. Selective area growth of GaN nanowires and nanofins by molecular beam epitaxy on heteroepitaxial diamond (001) substrates. *Nanoscale Adv.* **2021**, *3*, 3835−3845.
(20) Gačević, Z.; Gómez Sánchez, D.; Calleja, E. Formation mechanisms of GaN nanowires grown by selective area growth homoepitaxy. *Nano Lett.* **2015**, *15*, 1117−1121.
(21) Li, G.; Yao, Y.; Dagenais, M. Selective area growth of GaN nanowires on Si (111) substrate with Ti masks by molecular beam epitaxy. *J. Cryst. Growth* **2019**, *524*, No. 125181.
(22) Kishino, K.; Hoshino, T.; Ishizawa, S.; Kikuchi, A. Selective-area growth of GaN nanocolumns on titanium-mask-patterned silicon (111) substrates by RF-plasma-assisted molecular-beam epitaxy. *Electron. Lett.* **2008**, *44*, 819−821.
(23) Hartmann, J.; Steib, F.; Zhou, H.; Ledig, J.; Nicolai, L.; Fündling, S.; Schimpke, T.; Avramescu, A.; Varghese, T.; Trampert, A.; Straßburg, M.; Lugauer, H. J.; Wehmann, H. H.; Waag, A. Study of 3D-growth conditions for selective area MOVPE of high aspect ratio GaN fins with non-polar vertical sidewalls. *J. Cryst. Growth* **2017**, *476*, 90−98.
(24) Lin, Y.-T.; Yeh, T.-W.; Dapkus, P. D. Mechanism of selective area growth of GaN nanorods by pulsed mode metalorganic chemical vapor deposition. *Nanotechnology* **2012**, *23*, No. 465601.
(25) Hartmann, J.; Steib, F.; Zhou, H.; Ledig, J.; Fündling, S. N.; Albrecht, F.; Schimpke, T.; Avramescu, A.; Varghese, T.; Wehmann, H.-H.; Straßburg, M.; Lugauer, H. J.; Waag, A. High aspect ratio GaN fin microstructures with nonpolar sidewalls by continuous mode metalorganic vapor phase epitaxy. *Cryst. Growth Des.* **2016**, *16*, 1458−1462.
(26) Schuster, F.; Hetzl, M.; Weiszer, S.; Garrido, J. A.; De La Mata, M.; Magen, C.; Arbiol, J.; Stutzmann, M. Position-controlled growth of GaN nanowires and nanotubes on diamond by molecular beam epitaxy. *Nano Lett.* **2015**, *15*, 1773−1779.
(27) Pantle, F.; Karlinger, M.; Wörle, S.; Becker, F.; Höldrich, T.; Sirotti, E.; Kraut, M.; Stutzmann, M. Crystal side facet-tuning of GaN nanowires and nanofins grown by molecular beam epitaxy. *J. Appl. Phys.* **2022**, *132*, 184304.
(28) Roshko, A.; Brubaker, M.; Blanchard, P.; Harvey, T.; Bertness, K. A. Selective area growth and structural characterization of GaN nanostructures on Si (111) substrates. *Crystals* **2018**, *8*, 366.
(29) Staudinger, P.; Moselund, K. E.; Schmid, H. Exploring the size limitations of wurtzite III−V film growth. *Nano Lett.* **2020**, *20*, 686−693.
(30) Yuan, X.; Pan, D.; Zhou, Y.; Zhang, X.; Peng, K.; Zhao, B.; Deng, M.; He, J.; Tan, H. H.; Jagadish, C. Selective area epitaxy of III−V nanostructure arrays and networks: Growth, applications, and future directions. *Appl. Phys. Rev.* **2021**, *8*, No. 021302.
(31) Zhang, Y.; Zubair, A.; Liu, Z.; Xiao, M.; Perozek, J.; Ma, Y.; Palacios, T. GaN FinFETs and trigate devices for power and RF applications: Review and perspective. *Semicond. Sci. Technol.* **2021**, *36*, No. 054001.
(32) Sekiguchi, H.; Kishino, K.; Kikuchi, A. Ti-mask selective-area growth of GaN by RF-plasma-assisted molecular-beam epitaxy for fabricating regularly arranged InGaN/GaN nanocolumns. *Appl. Phys. Express* **2008**, *1*, No. 124002.
(33) Li, H.; Geelhaar, L.; Riechert, H.; Draxl, C. Computing equilibrium shapes of wurtzite crystals: the example of GaN. *Phys. Rev. Lett.* **2015**, *115*, No. 085503.
(34) Van de Walle, C. G.; Segev, D. Microscopic origins of surface states on nitride surfaces. *J. Appl. Phys.* **2007**, *101*, No. 081704.
(35) Choi, S.; Kim, T.-H.; Everitt, H. O.; Brown, A.; Losurdo, M.; Bruno, G.; Moto, A. Kinetics of gallium adlayer adsorption/desorption on polar and nonpolar GaN surfaces. *J. Vac. Sci. Technol. B* **2007**, *25*, 969−973.
(36) Bertness, K. A.; Roshko, A.; Mansfield, L.; Harvey, T. E.; Sanford, N. A. Mechanism for spontaneous growth of GaN nanowires with molecular beam epitaxy. *J. Cryst. Growth* **2008**, *310*, 3154−3158.
(37) Consonni, V.; Dubrovskii, V.; Trampert, A.; Geelhaar, L.; Riechert, H. Quantitative description for the growth rate of self-induced GaN nanowires. *Phys. Rev. B* **2012**, *85*, No. 155313.
(38) Gridchin, V. O.; Dvoretckaia, L. N.; Kotlyar, K. P.; Reznik, R. R.; Parfeneva, A. V.; Dragunova, A. S.; Kryzhanovskaya, N. V.; Dubrovskii, V. G.; Cirlin, G. E. Selective area epitaxy of GaN nanowires on Si substrates using microsphere lithography: Experiment and theory. *Nanomaterials* **2022**, *12*, 2341.

https://doi.org/10.1021/acs.cgd.2c01506
Cryst. Growth Des. 2023, 23, 4098−4104